A Numerical Investigation on a Caloric Heat Pump Employing Nanofluids

Ciro Aprea[1], Adriana Greco[2], Angelo Maiorino[1], Claudia Masselli[1*]

[1] DIIn, University of Salerno, Via Giovanni Paolo II, 132 Fisciano (SA) 84084, Italy
[2] DII, University of Naples "Federico II", P.le Tecchio 80, Napoli 80125, Italy

Corresponding Author Email: cmasselli@unisa.it

ABSTRACT

Nowadays vapor compression is still the reference technique for heat pumping applications. There are Not-In-Kind heat pumping technologies where a prominent role is occupied by the ones based on solid-state refrigerants, called caloric. The name of such class of technologies comes from caloric effect, manifesting in caloric materials as temperature change due to an applied external field which changes its intensity adiabatically. The reference thermodynamical cycle is called Active Caloric Regenerative heat pump (ACR) cycle and it is applied to a caloric solid-state structure which is both refrigerant and regenerator. The structure is crossed by a Heat Transfer Fluid (HTF) (generally water) that transfers heat from the cold to the hot environment. This paper proposes optimizing solutions as nanofluids for enhancing the heat transfer. The energy performances of a caloric heat pump employing Al_2O_3-water nanofluids as HTF are evaluated through a 2-D model, for a wide set of caloric materials. The investigation reveals that the addition of nanofluids carries to an upgrade of the energy performances of the heat pump. The best combination occurs if the heat pump works with Ni-Ti (as refrigerant) and alumina-water nanofluid (10 % vol) as HTF.

1. INTRODUCTION

Nowadays vapor compression is still considered the reference technique for cooling and heat pumping applications [1, 2]. Over the last 20 years vapor compression is going through years of profound renewal [3, 4], due to the damages in terms of ozone depletion and global warming, provoked by the employment of fluid refrigerants [5-7]. Parallelly to the countermeasures adopted to limit the damage caused by vapor compression [8-13], alternative solutions to it are also being sought [14]. There are the cooling and heat pumping technologies, defined as Not-In-Kind [15, 16] where a prominent role is occupied by the class based on solid-state refrigerants, called caloric [17-20]. The name of such class of technologies comes from caloric effect: an intrinsic property of ferroic materials manifesting as temperature change due to an applied external field which changes its intensity adiabatically [21]. If the variation occurs isothermally, a total entropy change is detected in the material. These two variations are regulated by:

$$\Delta s = \int_{Y_0}^{Y_1} \left(\frac{\partial X}{\partial T}\right)_Y dY \qquad (1)$$

$$\Delta T_{ad} = -\int_{Y_0}^{Y_1} \frac{T}{C}\left(\frac{\partial X}{\partial T}\right)_Y dY \qquad (2)$$

The nature of the driving field Y particularizes the caloric effect. Magnetic fields applied to magnetocaloric materials give rise to magnetocaloric effect (MCE) [22, 23] where Y=H and X=M, electric fields to electrocaloric effect (ECE) [24] where Y=E and X=P, mechanical stress to elastocaloric effect (eCE) [25], where Y=σ and X=ε, pressure field to barocaloric effect (BCE) [26] where Y=- p and X=V.

The reference thermodynamical cycle of a caloric heat pump is called Active Caloric Regenerative heat pump (ACR) cycle and it is based on a Brayton cycle [27]. The ACR cycle is applied to a caloric solid-state structure which is both refrigerant and regenerator. The structure is placed between a cold and a hot heat exchanger and it is subjected to alternative cycles of intensity increasing/decreasing of the applied field. Therefore, the refrigerant has a solid-state but an auxiliary fluid (generally water or water-glycol mixture) is used to transfer the fluxes between the hot and the cold heat exchangers; thus, it is called Heat Transfer Fluid (HTF).

The four processes identifying the ACR cycle are the following:

1) adiabatic decreasing of the intensity of the external field applied to the caloric structure whom, consequently, cools down following caloric effect;

2) the cooled down caloric structure absorbs heat from the HTF that crosses it from the hot to the cold side.

3) adiabatic increasing of the intensity of the external field applied to caloric structure whom, as a consequence, heats up due to caloric effect;

4) the heat exchanged is pumped toward the environment by means of HTF flowing in the hot heat exchanger from the cold to the hot side of the regenerator. Indeed, the heat transfer fluid reaches the hot side (connected to the environment to be heat pumped) hotter than the medium temperature of the hot heat exchanger. Consequently, the fluid adduces heat toward the environment, and it realizes the desired effect of the ACR cycle for heat pumping.

As mentioned before, generally, the secondary heat-transfer fluid is water or a water-ethylene mixture for sub-zero applications. Since the auxiliary fluid is responsible of the heat transferring in the regenerator from a side to another,

optimizing solutions should be proposed for enhancing the heat transfer between the solid-state refrigerant and the fluid itself. One of these is constituted by nanofluids [28, 29].

Nanofluids are classified as new kind of heat transfer fluids; they are formed by common base fluids in which are dispersed solid-state nanoparticles due of high thermal conductivity. The nanoparticles, as the name suggests, present nanometric dimensions (<100 nm) and they could have metallic or non-metallic nature. The resulting fluid is a stable mixture of a base-fluid with nanoparticles, called nanofluid, due of enhanced thermal conductivity with respect to the starting base-fluid [30, 31]. Nanofluids were presented for the first time to scientific community in 1995 by Choi [32] but, given the revolutionary discovered, they gained much attentions and all over the world scientists started to test nanofluids in the most varied applications [33-39].

As regards to solid-state refrigeration, very few have been studies on the application on nanofluids in the caloric systems and some of them are focused on magnetocaloric refrigeration [40-42]. The study on working with nanofluids in the other caloric-effects-based heat pumping systems is still an unexplored field, except the work proposed by Greco et al. [43] where the energy performances of a caloric heat pump employing Al_2O_3 + water nanofluids as HTF are evaluated. The present paper aims to expand the above-mentioned analysis, evaluating the significative energy parameters. The investigation is perpetuated through a two-dimensional model, previously experimentally validated [44, 45] with a rotary prototype [46, 47]. The tests were performed changing both the nanoparticle volume fraction of the nanofluids and the caloric materials, testing electrocaloric, elastocaloric and barocaloric candidates.

2. THE STEPS OF THE INVESTIGATION

This section aims to describe the salient steps of the investigation as: the choice of the caloric materials and the nanofluids; the description of the 2-D numerical tool employed for the investigation; the way the properties of the nanofluids and the caloric effect materials were modeled in the tool.

2.1 Caloric solid-state refrigerants

To select the caloric refrigerants for the present investigation we based on high-caloric effects and diversity criteria, in order to test the most performing ones, in room temperature range, among the electrocaloric, elastocaloric and barocaloric effect materials.

$Pb_{0.97}La_{0.02}(Zr_{0.75}Sn_{0.18}Ti_{0.07})$ O_3 (PLZST) [48], deposited on $LaNiO_3/Si$ (100) substrate, is the electrocaloric material under test. It exhibits a maximum Giant ECE at 278 K but ΔT_{ad} remains very high in the range 278÷298 K, making PLZST suitable for heat pump applications. Specifically, we considered it under electric field changes of 90 MV m^{-1} and 70 MV m^{-1} whose peaks of ΔT_{ad} are 54 K and 43 K, respectively.

We also considered the elastocaloric Ni-Ti polycrystals [49], benchmark of elastocaloric systems, showing a peak at 350 K but anyway exhibiting a remarkable elastocaloric effect in temperature range devoted to heat pump applications. The considered stress field change is 0.9 GPa

which results in a peak of 25 K as adiabatic temperature change due to elastocaloric effect.

The barocaloric oxyfluorides $(NH_4)_2MoO_2F_4$ [50] showing a maximum direct barocaloric effect at 272 K which remains remarkable until 360 K, ensures a good applicability for heat pumps operation mode. The considered drop of applied pressure field is 0.9 GPa that guarantees a maximum of 18 K due to barocaloric effect.

As barocaloric we also focused on Acetoxy Silicone Rubber (ASR) exhibiting a supergiant [51] barocaloric effect investigated for Δp=[0.273; 0.390] GPa under which associated maximums ΔT_{ad} of 30 and 41 K occur, respectively.

2.2 The heat transfer nanofluids

In the present investigation the considered heat transfer fluids are the alumina–water nanofluids. They are composed of water, as base fluid, in which nanometric particles of alumina (Al_2O_3) were dispersed.

Table 1 lists the properties of the base fluid and the nanoparticles of alumina-water nanofluids at T=293 K and p=1 atm.

Table 1. Thermophysic properties of the base fluid the and nanoparticles of the alumina-water nanofluids

Substance	ρ $\left[\frac{kg}{m^3}\right]$	C $\left[\frac{J}{kgK}\right]$	k $\left[\frac{W}{mK}\right]$	μ $\left[\frac{kg}{ms}\right]$
Water	998.2	4182	0.597	9.93*10^{-4}
Al_2O_3	3970	765	36	-

The thermophysical properties of the nanofluids were evaluated through the following mathematical correlations available in open scientific literature [52-54]:

$$\rho_{nf} = (1 - \varphi)\,\rho_{bf} + \varphi\,\rho_{np} \tag{3}$$

$$\rho_{nf}C_{p,nf} = (1 - \varphi)(\rho C_p)_{bf} + \varphi\,(\rho C_p)_{np} \tag{4}$$

$$\mu_{nf} = \mu_{bf}(1 + 7.74\varphi) \tag{5}$$

$$k_{nf} = k_{bf}\,\frac{k_{np}+2k_{bf}-2\varphi(k_{bf}-k_{np})}{k_{np}+2k_{bf}+\varphi(k_{bf}-k_{np})} \tag{6}$$

where, φ is the volume fraction of the nanoparticles dispersed on equal volume of base fluid as:

$$\varphi = \frac{V_{np}}{V_{nf}} = \frac{m_{np}}{m_{nf}} \tag{7}$$

2.3 The 2-D model of a caloric heat pump

The behavior of a caloric heat pump is described through a 2-D model, already introduced [19] and validated experimentally in previous investigations [44, 45]. The geometry of the heat pump sees a parallel-plate regenerator made of caloric material, separated by channels in which the HTF crosses the regenerator. The desired effect is to add heat to the indoor room connected with a hot heat exchanger at T_H. The cold heat exchanger is coupled with the outdoor environment, whose temperature is T_C. Below there is the mathematical structure that the 2-D model is based on:

$$\begin{cases} \dfrac{\partial u}{\partial x} + \dfrac{\partial v}{\partial y} = 0 \\[6pt] \dfrac{\partial u}{\partial t} + u\dfrac{\partial u}{\partial x} + v\dfrac{\partial u}{\partial y} = -\dfrac{1}{\rho_{nf}}\dfrac{\partial p}{\partial x} + \nu\left(\dfrac{\partial^2 u}{\partial x^2} + \dfrac{\partial^2 u}{\partial y^2}\right) \\[6pt] \dfrac{\partial v}{\partial t} + u\dfrac{\partial v}{\partial x} + v\dfrac{\partial v}{\partial y} = -\dfrac{1}{\rho_{nf}}\dfrac{\partial p}{\partial y} + \nu\left(\dfrac{\partial^2 v}{\partial x^2} + \dfrac{\partial^2 v}{\partial y^2}\right) \\[6pt] \dfrac{\partial T_{nf}}{\partial t} + u\dfrac{\partial T_{nf}}{\partial x} + v\dfrac{\partial T_{nf}}{\partial y} = \dfrac{k_f}{\rho_{nf}C_{nf}}\left(\dfrac{\partial^2 T_{nf}}{\partial x^2} + \dfrac{\partial^2 T_{nf}}{\partial y^2}\right) \\[6pt] \dfrac{\partial T_S}{\partial t} = \dfrac{k_s}{\rho_s C_s}\left(\dfrac{\partial^2 T_S}{\partial x^2} + \dfrac{\partial^2 T_S}{\partial y^2}\right) \end{cases} \quad (8)$$

$$\begin{cases} \rho_{nf}C_{nf}\dfrac{\partial T_{nf}}{\partial t} = k_{nf}\left(\dfrac{\partial^2 T_{nf}}{\partial x^2} + \dfrac{\partial^2 T_{nf}}{\partial y^2}\right) \\[6pt] \rho_s C_s \dfrac{\partial T_S}{\partial t} = k_s\left(\dfrac{\partial^2 T_S}{\partial x^2} + \dfrac{\partial^2 T_S}{\partial y^2}\right) + Q \end{cases} \quad (9)$$

$$Q = Q(field, T_S) = \frac{\rho_s\, C_s(field, T_S)\Delta T_{ad}(field, T_S)}{\tau} \quad (10)$$

Eq. (8) models the fluid-flow processes of the ACR cycle; Eq. (9) describes the field rising/falling phases. Caloric effect is modeled through the Q-term reported in Eq. (10). It converts the caloric effect into a power density. Since Q is a function of the field and the temperature, its mathematical expression was obtained by a mathematical finder software, as a result of elaboration and manipulation of experimental data of C_s (field, T_s) and ΔT_{ad} (field, T_s), coming from scientific literature. Different Q-terms correspond to the tested caloric materials.

The model is solved with Finite Element Method and the ACR cycle runs cyclically several times until reaching steady state that is satisfying the cyclicality criterion in every point the ACR regenerator:

$$\delta = max\{T(x, y, 0 + n\theta) - T(x, y, 4\tau + n\theta)\} < \bar{\varepsilon} \quad (11)$$

3. METHODOLOGY OF THE INVESTIGATION

We tested the caloric materials introduced in section 2.1 as refrigerants of the active solid-state heat pump modelled by the 2-D model. The heat pump was supposed to work in the range $T_C \div T_H$ = 278÷298 K at 1.25 Hz and 0.2 m s^{-1}, respectively as ACR cycle and nanofluid velocity. The alumina-water nanofluid with nanoparticles volume fraction varied in the range 0÷10 % was employed in the heat pump as heat transfer fluid.

The most significative energy performance carried out are introduced below.

An outstanding parameter is the ACR temperature span evaluated as:

$$\Delta T_{ACR} = \frac{1}{\tau}\int_{\tau+n\theta}^{2\tau+n\theta} T_{nf}(L, y, t)dt - \frac{1}{\tau}\int_{3\tau+n\theta}^{4\tau+n\theta} T_{nf}(0, y, t)\,dt \quad (12)$$

ΔT_{ACR} is a parameter used to evaluate the maximum temperature drop across the ACR since it measures the temperature difference between the nanofluid exiting the regenerator at the hot side ($x = L$) during the cold-to-hot flowing phase and at the cold side (x = 0) during the hot-to cold flowing phase.

Another remarkable parameter is the power of the heat pump, that measures the power at which the system pumps heat:

$$\dot{Q}_{H} = \frac{1}{\theta}\int_{\tau+n\theta}^{2\tau+n\theta} \dot{m}_{nf}C_{nf}(T_{nf}(L, y, t) - T_{H})\,dt \quad (13)$$

The Coefficient of Performance (COP) is conceived as the ratio between the heating power of the pump and the total energy spent to get it:

$$COP = \frac{\dot{Q}_{H}}{\dot{W}_{TOT}} = \frac{\dot{Q}_{H}}{\dot{W}_{field} + \dot{W}_{pump}} \quad (14)$$

$\dot{W}_{TOT}$ embraces both the contribution due to the external field variation ($\dot{W}_{field}$) and the one connected to the mechanical power required for the fluid motion ($\dot{W}_{pump}$), defined as follows:

$$\dot{W}_{field} = \dot{Q}_{H} - \dot{Q}_{ref} \quad (15)$$

$$\dot{W}_{pump} = \frac{\dot{m}_{nf}(\Delta p_{CF} + \Delta p_{HF})}{\eta_p \rho_{nf}} \quad (16)$$

4. RESULTS

Basing on the methodology and the working conditions introduced in section 3, the most salient parameters to evaluate the energy performances of the caloric heat pump, were carried out and the results are reported in the present section.

Figure 1 reports the ACR temperature span as a function of nanoparticle volume fraction, for the set of the caloric materials tested. The results reveal that the highest temperature drops are proper of the electrocaloric PLZST for both the ΔE considered. The absolute maximum is greater than 70 K and it has been detected when the regenerator works with PLZST under ΔE=90 MV m^{-1} as solid-state refrigerant and with Al$_2$O$_3$-water nanofluid (10 % vol) as HTF. All the materials exhibiting a mechanocaloric effect (elastocaloric or barocaloric) present ΔT_{ACR} belonging to 30÷40 K range. Among them the best ΔT_{ACR} are the ones provided by ASR under Δp = 390 GPa. The addiction of nanofluids brings to an increasing of ACR temperature span, with augmenting φ, for all the tested materials. A maximum increment of +4.2 % has been observed for the elastocaloric NiTi, if the nanoparticle volume fraction of the alumina-water nanofluids grows from 0 % up to 10 %. Considering globally the whole set of the caloric materials under test, the medium benefit registered if the regenerator works with nanofluids, in terms of ΔT_{ACR} is an increament of +3.4 %.

Avoid writing long formulas with subscripts in the title; short formulas that identify the elements are fine (e.g., "Nd–Fe–B").

Figure 2 shows the heating power of the caloric heat-pump for the tested materials occurring under the operative conditions of section 3, when the heat-transfer fluid is alumina-water based nanofluid with variable concentration. General considerations arising through the examination of the data plotted are that $\dot{Q}_{H}$ increases with φ for all the tested materials. The medium benefit toward this parameter translates in a medium increment of +19 % if the system works with nanofluids. Specifically, PLZST under ΔE=90 MV m^{-1} as well as NiTi under Δσ=0.9 GPa provide the highest $\dot{Q}_{H}$ with a maximum settled around 580 W if the nanoparticle volume fraction of the alumina-water nanofluid is 10 %. This is due to the Giant ECE shown at 278 K by the

former, and to the fact that elastocaloric effect is quite constant in the considered temperature range. On the contrary the lowest heating-powers are detected for $(NH_4)_2MoO_2F_4$ since they do not exceed 240 W. Such results are due both to the ΔT_{ad} smaller than PLZST ones and to the peak located at 272 K (out of the working temperature range).
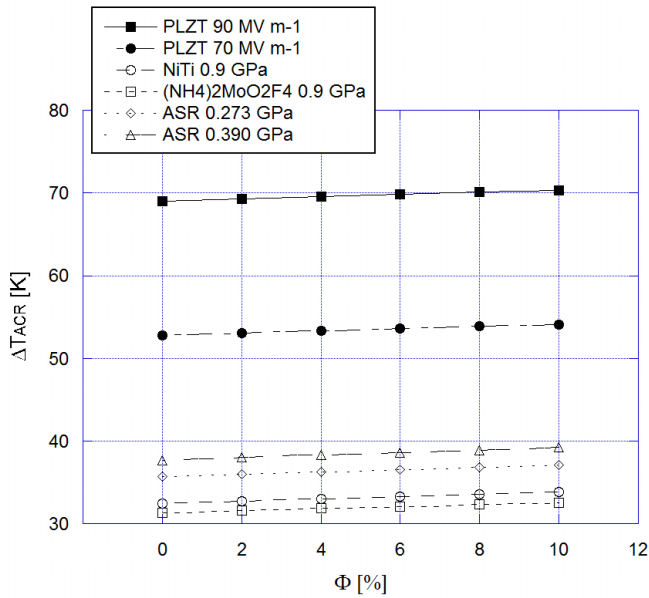

Figure 1. ΔT_{ACR} as a function of nanoparticles volume fraction, evaluated for the set of the caloric materials under test
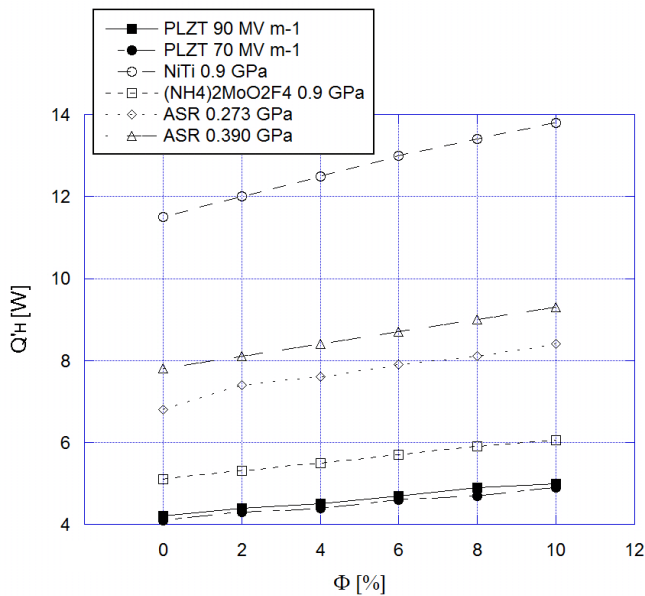

Figure 2. $\dot{Q}_H$ as a function of nanoparticles volume fraction, evaluated for the set of the caloric materials under test

Figure 3 reports the coefficients of performances of the set of the caloric materials under test. COP has been reported with respect to the nanoparticle volume fraction of the alumina-water nanofluids. The situation is quite different from the data about heat-pumping powers, since the material with highest-COPs is still NiTi but not anymore PLZST. The latter exhibits, for both the 90 MV m^{-1} and 70 MV m^{-1} electric field variations, the lowest coefficients of performances of the set of tested materials. Such turnarounds

are caused by the expenses needed for large electric field changing, resulting higher than mechanical stretching ones. The NiTi based caloric heat pump presents 14.8 as maximum COP, if it works with 10 % alumina-90 % water nanofluid. A middle COP-increment of +15 % is detected if the nanofluid concentration increases from 0% up to 10 %. The barocaloric Acetoxy Silicone Rubber presents also satisfying COPs with a maximum of 9.3 registered for φ=0.1 under Δp=0.39 GPa and a middle increment of +19 % while increasing nanoparticle volume fraction.
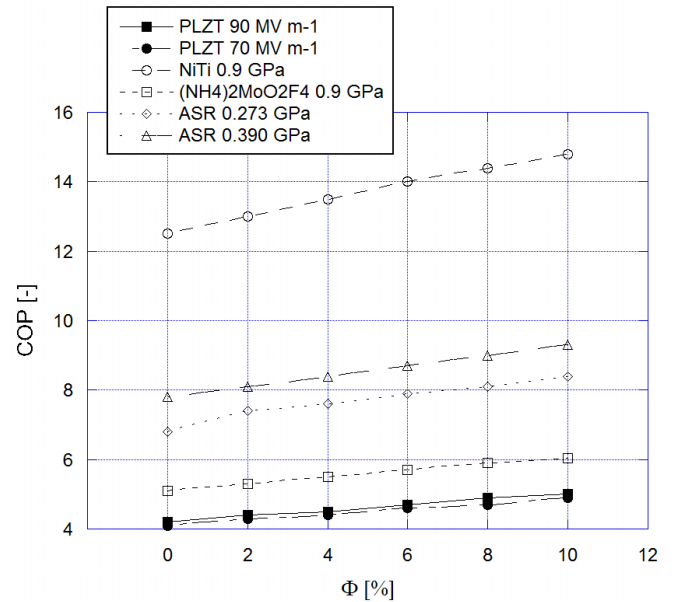

Figure 3. Coefficient of performance as a function of nanoparticles volume fraction, evaluated for the set of the caloric materials under test
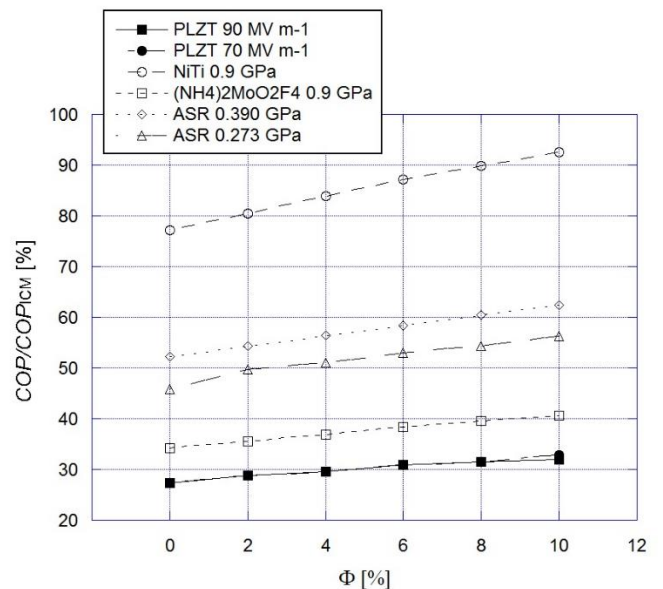

Figure 4. COP on Carnot COP as a function of nanoparticles volume fraction, evaluated for the set of the caloric materials under test

Furthermore, in Figure 4 the obtained coefficients of performance are compared to the Carnot COP. The material that comes closest to the Carnot COP is the elastocaloric NiTi with values mediumly around 85 % of it. Specifically,

the addiction of alumina-water nanofluids takes the COP of NiTi from 78 % (with $\varphi=0$) up to 92 % (with $\varphi=10$ %).

On the contrary, due to the high expense required to generate the considered electric fields, the electrocaloric PLZST shows coefficients of performance just around 28 % of ICM, with $\varphi=0$. Not even the employment of nanofluids leads to a significant increase, since the maximum COP/COP_{ICM} achieved is 35 % (under $\varphi=10$ %). Anyhow, as general comment, the addiction of nanofluids has a positive increment on the coefficients of performance of each material tested, that come closer to the COP_{ICM} of +20 % (as average data) if $\varphi=10$ %, with respect of the regenerator employing the base fluid as HTF ($\varphi=0$ %).

5. CONCLUSIONS

This paper proposes optimizing solutions as nanofluids for enhancing the heat transfer. The energy performances of a caloric heat pump employing Al_2O_3-water nanofluids as HTF were evaluated through a 2-D model, for a wide set of caloric materials. The investigation reveals that the addition of nanofluids carries to an upgrade of the energy performances of the heat pump.

In terms of ΔT_{ACR}, the best performances are proper of the electrocaloric PLZST for both the ΔE considered with an absolute maximum greater than 70 K, detected under $\Delta E=90 MV\ m^{-1}$ and $\varphi=10$ %. Considering globally the whole set of the caloric materials under test, the medium benefit registered if the regenerator works with nanofluids, in terms of ΔT_{ACR} is an increment of +3.4 %.

The highest heat pumping powers were noticed for PLZST under $\Delta E=90\ MV\ m^{-1}$ as well as NiTi under $\Delta\sigma=0.9\ GPa$. Considering the while set of tested materials, the medium benefit toward this parameter translates in a medium increment of +19 % if the system works with nanofluids.

The material with highest-COPs is still NiTi but not anymore PLZST, whose COPs are the lowest due to the high expense required for varying the intensity of the electric field. The material that comes closest to the Carnot COP is the elastocaloric NiTi with values mediumly around 85 % of it. Anyhow, as general comment, the addiction of nanofluids has a positive increment on the coefficients of performance of each material tested, that come closer to the COP_{ICM} of +20 % (as average data) if $\varphi=10$ %, with respect of the regenerator employing the base fluid as HTF ($\varphi=0$ %).

Therefore, basing on the results presented one can conclude that the best combination occurs if the caloric heat pump works with Ni-Ti as refrigerant, and alumina-water nanofluid (10 % vol) as heat transfer fluid.

REFERENCES

[1] Moretti, E., Nassuato, L., Bordoni, G.P. (2019). Development of regression models to predict energy consumption in industrial sites: The case study of a manufacturing company in the central Italy. Tecnica Italiana - Italian Journal of Engineering Science, 63(2-4): 343-348. https://doi.org/10.18280/ti-ijes.632-433

[2] Ahamed, J.U., Saidur, R., Masjuki, H.H. (2011). A review on exergy analysis of vapor compression refrigeration system. Ren. and Sust. En. Rev., 15(3): 1593-1600. https://doi.org/10.1016/j.rser.2010.11.039

[3] Montreal Protocol on substances that deplete the ozone layer, United Nation Environment Program (UN), New York, NY, USA, 1987.

[4] Heath, E.A. (2017). Amendment to the Montreal protocol on substances that deplete the ozone layer (Kigali Amendment). Int. Legal Mater., 56(1): 193-205 https://doi.org/10.1017/ilm.2016.2

[5] Greco, A., Vanoli, G.P. (2005). Flow boiling heat transfer with HFC mixtures in a smooth horizontal tube. Part II: Assessment of predictive methods. Experimental Thermal and Fluid Science, 29(2): 199-208. https://doi.org/10.1016/j.expthermflusci.2004.03.004

[6] Calm, J.M., Didion, D.A. (1998). Trade-offs in refrigerant selections: past, present, and future. Int. J. of Refrig., 21(4): 308-321. https://doi.org/10.1016/S0140-7007(97)00089-3

[7] Greco, A., Mastrullo, R., Palombo, A. (1997). R407C as an alternative to R22 in vapour compression plant: An experimental study. Int. J. of En. Res., 21(12): 1087-1098. https://doi.org/10.1002/(SICI)1099-114X(19971010)21:12<1087::AID-ER330>3.0.CO;2-Y

[8] Abas, N., Kalair, A.R., Khan, N., Haider, A., Saleem, Z., Saleem, M.S. (2018). Natural and synthetic refrigerants, global warming: A review. Ren. and Sust. En. Rev., 90: 557-569. https://doi.org/10.1016/j.rser.2018.03.099

[9] Aprea, C., Greco, A., Maiorino, A., Masselli, C., Metallo, A. (2016). HFO1234ze as drop-in replacement for R134a in domestic refrigerators: An environmental impact analysis. En. Proc., 101: 964-971. https://doi.org/10.1016/j.egypro.2016.11.122

[10] McLinden, M.O., Brown, J.S., Brignoli, R., Kazakov, A.F., Domanski, P.A. (2017). Limited options for low-global-warming-potential refrigerants. Nature Communications, 8: 14476. https://doi.org/10.1038/ncomms14476

[11] Aprea, C., Greco, A., Maiorino, A., Masselli, C., Metallo, A. (2016). HFO1234yf as a drop-in replacement for R134a in domestic refrigerators: A life cycle climate performance analysis. Int. J. of Heat and Techn., 34(2): S212-S218. https://doi.org/10.18280/ijht.34S204

[12] Bolaji, B.O., Huan, Z. (2013). Ozone depletion and global warming: Case for the use of natural refrigerant– a review. Ren. and Sust. En. Rev., 18: 49-54. https://doi.org/10.1016/j.rser.2012.10.008

[13] Aprea, C., Greco, A., Maiorino, A., Masselli, C. (2018). The drop-in of HFC134a with HFO1234ze in a household refrigerator. Int. J. of Therm. Sc., 127: 117-125. https://doi.org/10.1016/j.ijthermalsci.2018.01.026

[14] Brown, J.S., Domanski, P.A. (2014). Review of alternative cooling technologies. Appl. Therm. Eng., 64(1-2): 252-262.10. https://doi.org/1016/j.applthermaleng.2013.12.014

[15] Bansal, P., Vineyard, E., Abdelaziz, O. (2012). Status of not-in-kind refrigeration technologies for household space conditioning, water heating and food refrigeration. Int. J. of Sust. Built Env., 1(1): 85-101. https://doi.org/10.1016/j.ijsbe.2012.07.003

[16] Qian, S., Nasuta, D., Rhoads, A., Wang, Y., Geng, Y., Hwang, Y., Radermacher, R., Takeuchi, I. (2016). Not-in-kind cooling technologies: A quantitative comparison of refrigerants and system performance. Int. J. of Refrig.,

62: 177-192. https://doi.org/10.1016/j.ijrefrig.2015.10.019

[17] Aprea, C., Greco, A., Maiorino, A., Masselli, C. (2017). Electrocaloric refrigeration: an innovative, emerging, eco-friendly refrigeration technique. J. of Phys.: Conf. Ser., 796(1): 012019. https://doi.org/10.1088/1742-6596/796/1/012019

[18] Kitanovski, A., Plaznik, U., Tomc, U., Poredoš, A. (2015). Present and future caloric refrigeration and heat-pump technologies. Int. J. of Refrig., 57: 288-298. https://doi.org/10.1016/j.ijrefrig.2015.06.008

[19] Aprea, C., Greco, A., Maiorino, A., Masselli, C. (2018). Solid-state refrigeration: A comparison of the energy performances of caloric materials operating in an active caloric regenerator. Energy, 165: 439-455. https://doi.org/10.1016/j.energy. 2018.09.114

[20] Greco, A. Aprea, C., Maiorino, A., Masselli, C. (2019). A review of the state of the art of the solid-state caloric cooling processes at room-temperature before 2019. Int. J. of Refrig., 106: 66-88. https://doi.org/10.1016/j.ijrefrig.2019.06.034

[21] Fähler, S., Rößler, U. K., Kastner, O., Eckert, J., Eggeler, G., Emmerich, H., Entel P., Müller S., Quandt E., Albe, K. (2012). Caloric effects in ferroic materials: New concepts for cooling. Adv. Eng. Mat., 14(1-2): 10-19. https://doi.org/10.1002/adem.201100178

[22] Aprea, C., Greco, A., Maiorino, A. (2013). The use of the first and of the second order phase magnetic transition alloys for an AMR refrigerator at room temperature: A numerical analysis of the energy performances. En. Conv. and Man., 70: 40-55. https://doi.org/10.1016/j.enconman.2013.02.006

[23] Aprea, C., Greco, A., Maiorino, A., Masselli, C. (2015). A comparison between rare earth and transition metals working as magnetic materials in an AMR refrigerator in the room temperature range. Appl. Therm. Eng., 91: 767-777. https://doi.org/10.1016/j.applthermaleng.2015.08.083

[24] Aprea, C., Greco, A., Maiorino, A., Masselli, C. (2017). A comparison between electrocaloric and magnetocaloric materials for solid state refrigeration. Int. J. of Heat and Techn., 35(1): 225-234. https://doi.org/10.18280/ijht.350130

[25] Tušek, J., Engelbrecht, K., Millán-Solsona, R., Mañosa, L., Vives, E., Mikkelsen, L.P., Pryds, N. (2015). The elastocaloric effect: A way to cool efficiently. Adv. En. Mat., 5(13). https://doi.org/10.1002/aenm.201500361

[26] Strässle, T., Furrer, A., Dönni, A., Komatsubara, T. (2002). Barocaloric effect: The use of pressure for magnetic cooling in Ce3Pd20Ge6. J. of Appl. Phys., 91(10): 8543-8545. https://doi.org/10.1063/1.1456450

[27] Gómez, J.R., Garcia, R.F., Catoira, A.D.M., Gómez, M.R. (2013). Magnetocaloric effect: A review of the thermodynamic cycles in magnetic refrigeration. Ren. and Sust. En. Rev., 17: 74-82. https://doi.org/10.1016/j.rser.2012.09.027

[28] Saidur, R., Leong, K.Y., Mohammad, H. (2011). A review on applications and challenges of nanofluids. Ren. and Sust. En. Rev., 15(3): 1646-1668. https://doi.org/10.1016/j.rser.2010.11.035

[29] Kumar D., Sokhal G.S., Sharma P. (2019). Numerical analysis of the heat and fluids flow performance of CuO-nanofluids in flat tube with bend. Revue des Composites et des Materiaux Avances, 29(1): 63-69. https://doi.org/10.18280/rcma.290110

[30] Choi, S.U.S., Zhang, Z.G., Yu, W., Lockwood, F.E., Grulke, E.A. (2001). Anomalously thermal conductivity enhancement in nanotube suspensions. Appl. Phys. Lett., 79: 2252-2254. https://doi.org/10.1063/1.1408272

[31] Alirezaie, A., Hajmohammad, M.H., Alipour, A. (2018). Do nanofluids affect the future of heat transfer? A benchmark study on the efficiency of nanofluids. Energy, 157: 979-989. https://doi.org/10.1016/j.energy.2018.05.060

[32] Choi, S.U.S. (1995). Enhancing thermal conductivity of fluids with nanoparticles. Developments and Applications of Non-Newtonian Flows, FED, 231/MD 66: 99-105.

[33] Sharafeldin, M.A., Gróf, G., Mahian, O. (2017). Experimental study on the performance of a flat-plate collector using WO3/Water nanofluids. Energy, 141: 2436-2444. https://doi.org/10.1016/j.energy.2017.11.068

[34] Abadeh, A., Rejeb, O., Sardarabadi, M., Menezo, C., Passandideh-Fard, M., Jemni, A. (2018). Economic and environmental analysis of using metal-oxides/water nanofluid in photovoltaic thermal systems (PVTs). Energy, 159: 1234-1243. https://doi.org/10.1016/j.energy.2018.06.089

[35] Manikandan, S., Rajan, K.S. (2016). Sand-propylene glycol-water nanofluids for improved solar energy collection. Energy, 113: 917-929. https://doi.org/10.1016/j.energy.2016.07.120

[36] Krishnan, R.Y., Manikandan, S., Suganthi, K.S., Vinodhan, V.L., Rajan, K.S. (2016). Novel copper–Propylene glycol nanofluid as efficient thermic fluid for potential application in discharge cycle of thermal energy storage. Energy, 107: 482-492. https://doi.org/10.1016/j.energy.2016.04.047

[37] Kazemi-Beydokhti, A., Heris, S.Z. (2012). Thermal optimization of combined heat and power (CHP) systems using nanofluids. Energy, 44(1): 241-247. https://doi.org/10.1016/j.energy.2012.06.033

[38] Garoosi, F., Hoseininejad, F., Rashidi, M.M. (2016). Numerical study of natural convection heat transfer in a heat exchanger filled with nanofluids. Energy, 109: 664-678. https://doi.org/10.1016/j.energy.2016.05.051

[39] Chandrasekaran, P., Cheralathan, M., Kumaresan, V., Velraj, R. (2014). Enhanced heat transfer characteristics of water based copper oxide nanofluid PCM (phase change material) in a spherical capsule during solidification for energy efficient cool thermal storage system. Energy, 72: 636-642. https://doi.org/10.1016/j.energy.2014.05.089

[40] Chiba, Y. (2017). Enhancements of thermal performances of an active magnetic refrigeration device based on nanofluids. Mechanics, 23(1): 31-38. https://doi.org/10.5755/j01.mech.23.1.13452

[41] Mugica, I., Roy, S., Poncet, S., Bouchard, J., Nesreddine, H. (2017). Exergy analysis of a parallel-plate active magnetic regenerator with nanofluids. Entropy, 19(9): 464. https://doi.org/10.3390/e19090464

[42] Greco, A., Aprea, C., Maiorino, A., Masselli, C. (2019). On the utilization of nanofluids as secondary fluid for heat transfer in a magnetocaloric cooler. Tecnica Italiana – Italian Journal of Engineering Science, 63(1): 52-58. https://doi.org/10.18280/ti-ijes.630107

[43] Greco, A., Aprea, C., Maiorino, A., Masselli, C. (2019). Nanofluids as heat transfer fluids for high-efficiency caloric heat pumps. Tecnica Italiana – Italian Journal of Engineering Science, 63(2-4): 251-256. https://doi.org/10.18280/ti-ijes.632-419

[44] Aprea, C., Cardillo, G., Greco, A., Maiorino, A., Masselli, C. (2015). A comparison between experimental and 2D numerical results of a packed-bed active magnetic regenerator. Appl. Therm. Eng., 90: 376-383. https://doi.org/10.1016/j.applthermaleng.2015.07.020

[45] Aprea, C., Greco, A., Maiorino, A., Masselli, C. (2018). Energy performances and numerical investigation of solid-state magnetocaloric materials used as refrigerant in an active magnetic regenerator. Therm. Sc. and Eng. Progr., 6: 370-379. https://doi.org/10.1016/j.tsep.2018.01.006

[46] Aprea, C., Cardillo, G., Greco, A., Maiorino, A., Masselli, C. (2016). A rotary permanent magnet magnetic refrigerator based on AMR cycle. Appl. Therm. Eng., 101: 699-703. https://doi.org/10.1016/j.applthermaleng.2016.01.097

[47] Aprea, C., Greco, A., Maiorino, A. (2017). An application of the artificial neural network to optimise the energy performances of a magnetic refrigerator. Int. J. of Refrig., 82: 238-251. https://doi.org/10.1016/j.ijrefrig.2017.06.015

[48] Zhao, Y., Hao, X., Zhang, Q. (2015). A giant electrocaloric effect of a Pb 0.97 La 0.02 (Zr 0.75 Sn 0.18 Ti 0.07) O 3 antiferroelectric thick film at room temperature. J. of Mat. Chem. C, 3(8): 1694-1699. https://doi.org/10.1039/C4TC02381A

[49] Tušek, J., Engelbrecht, K., Millán-Solsona, R., Mañosa, L., Vives, E., Mikkelsen, L.P., Pryds, N. (2015). The elastocaloric effect: A way to cool efficiently. Adv. En. Mat., 5(13): 1500361. https://doi.org/10.1002/aenm.201500361

[50] Gorev, M.V., Bogdanov, E.V., Flerov, I.N., Kocharova, A.G., Laptash, N.M. (2010). Investigation of thermal expansion, phase diagrams, and barocaloric effect in the (NH 4) 2 WO 2 F 4 and (NH 4) 2 MoO 2 F 4 oxyfluorides. Phys. of the Sol. St., 52(1): 167-175. https://doi.org/10.1134/S106378341

[51] Imamura, W., Usuda, E.O., Paixão, L.S., Bom, N.M., Gomes, A.M., Carvalho, A.M.G. (2017). Supergiant barocaloric effects in acetoxy silicone rubber around room temperature. arXiv preprint arXiv:1710.01761

[52] Bianco, V., Vafai, K., Manca, O., Nardini, S. (2015). Heat transfer enhancement with nanofluids. CRC Press. https://doi.org/10.1201/b18324

[53] Brinkman, H.C. (1952). The viscosity of concentrated suspensions and solutions. The J. of Chemic. Phys., 20(4): 571. https://doi.org/10.1063/1.1700493

[54] Hamilton, R.L., Crosser, O.K. (1962) Thermal conductivity of heterogeneous two-component systems. Ind. & Eng. Chemis. Fund., 1(3): 187-191. https://doi.org/10.1021/i160003a005

NOMENCLATURE

C	specific heat, J. kg^{-1}. K^{-1}
E	electric field, V.m^{-1}
H	magnetic field, A. m^{-1}
k	thermal conductivity, W. m^{-1}. K^{-1}
L	length of the regenerator, m
M	magnetization, A. m^{-1}
m	mass, kg
P	polarization C. m^{-2}
p	pressure, Pa
Q	power density, W. m^{-3}
$\dot{Q}$	power, W
s	entropy, J. kg^{-1}. K^{-1}
T	temperature, K
t	time, s
u	longitudinal fluid velocity, m. s^{-1}
V	volume, m^3
v	orthogonal fluid velocity, m. s^{-1}
$\dot{W}$	mechanical power, W
X	conjugate field
x	longitudinal spatial coordinate, m
Y	applied driving field
y	orthogonal spatial coordinate, m

Greek symbols

Δ	finite difference
ε	elongation, %
θ	period of ACR cycle, s
μ	dynamic viscosity, kg. m^{-1}. s^{-1}
ν	cinematic viscosity, m^{+2}. s^{-1}
φ	nanofluid concentration
ρ	density, kg. m^{-3}
σ	stress, Pa
τ	period of each step of ACR cycle, s

Subscripts

0	initial
1	final
ad	adiabatic
bf	base fluid
C	cold
H	Hot
ICM	Inverse Carnot Machine
nf	nanofluid
np	nanoparticles
p	constant pressure
s	solid
TOT	total